Electronic Supplementary Material (ESI) for Journal of Materials Chemistry A.

Supplementary Information

Chromophore amphiphile-polyelectrolyte hybrid hydrogels for photocatalytic hydrogen production

Hiroaki Sai, Aykut Erbas, Adam Dannenhoffer, Dongxu Huang, Adam Weingarten, Erica Siismets, Kyujin Jang, Karen Qu, Liam C. Palmer, Monica Olvera de la Cruz, Samuel I. Stupp

Supplementary Discussion

Alternative pathways for incorporating PMIs into PEs

We attempted a number of alternative pathways to incorporate the PMI molecules into the covalent PE network to the one described in the main text. Polymerization in the presence of PMI molecules was only successful at very low concentration of PMIs due to the flocculation of the amphiphilic PMIs in the high concentration of APTAC in free radical polymerization conditions. Attempts to incorporate pre-assembled PMIs into these PE gels in aqueous environment were also unsuccessful (Figure S2), possibly because the pre-assembled PMIs were too large to penetrate through the mesh size of the covalent networks. The latter result indicate that if PMIs are assembled in the presence within the covalent hydrogels *via* solvent exchange from TFE to water and grow to significant length scales as they do in aqueous solution (micrometers), they are unlikely to escape the hydrogels at a significant diffusion rate due to entrapment within the covalent network. Indeed, these hybrid hydrogels retain the PMI supramolecular assemblies for at least two years within the PE networks while stored in both DI water as well as aqueous salt solutions. In contrast, hydrogels loaded with fluorescein sodium salt can retain the dye when the hydrogel is stored in DI water, but releases the fluorescein from the hydrogel once placed in salt solution (Figure S3). Since fluorescein does not form extended assemblies in water and has a carboxylate group that is negatively charged at neutral pH, the interaction between fluorescein molecules and the PE hydrogel network is primarily electrostatic in nature, which leads to its release in highly charge-screened environment. This difference indicates that the mechanism for persistent entrapment of the photocatalytic assemblies within the PE network is not only electrostatic in origin but steric as well. Indeed, the cryo-scanning electron microscopy images of the parent hydrogel and the corresponding hybrid hydrogels reveal sub-micrometer fractal structure of the covalent network, smaller than the ribbon sizes on the order

of a few micrometers (Figure S4). We also note that this approach for incorporation of CAs into PE hydrogels can be applied to other amphiphilic chromophore molecules, such as hydroxyl-terminated PMIs and 3-pentylamine-functionalized PMIs (Figure S5).

Loading of molybdenum-sulfur catalysts in PMI/PE hybrid hydrogels

When the monolithic hybrid hydrogels were placed in the solution of ascorbic acid and the molybdenum-sulfur catalyst, $Na_2[Mo_3S_{13}]$, and immediately irradiated with halogen lamps, hydrogen production turnover frequencies (TOFs) showed large variations between experiments and 1-3 order of magnitude lower than the previously reported PMI/poly(diallyldimethylammonium chloride) (PDDA) hydrogels.[7] We observed some samples with comparable TOFs when the hybrid hydrogels were broken in sub-millimeter sized pieces or freeze-dried and reconstituted before use. We thus hypothesized that the cause for reduced TOF was due to limited diffusion of components required for photocatalytic hydrogen production in the hydrogel network. Since the molybdenum-sulfur catalyst is a divalent anion with sodium counterions, we suspected that the catalyst can be prevented from infiltrating into a highly cationic covalent hydrogel network. This was confirmed by placing the parent APTAC dried gels into the $Na_2[Mo_3S_{13}]$ solution and observing the cross-section with optical microscopy, where the catalyst appears brown in color as a localized skin layer on the surface of the hydrogel (Figure S8). Dynamic light scattering (DLS) measurement of the $Na_2[Mo_3S_{13}]$ solution indeed showed that the catalyst tends to aggregate in aqueous solution (Figure S8). Therefore, in order to facilitate diffusive process of the catalyst into the hydrogels we performed all subsequent photocatalytic hydrogen production experiments by first adding the hybrid hydrogels with a known amount of catalyst solution and incubating the hydrogels at 75^{o}C prior to addition of the sacrificial electron donor reagent.

Kinetic study on photocatalytic hydrogen production

In order to prove the photocatalytic nature of the H_2 production, we performed gas chromatography on aliquoted headspace for vials containing the PMI/PE hybrid hydrogels and $Na_2[Mo_3S_{13}]$ catalyst in ascorbic acid solution under irradiation over time (Figure S10). While variations in placement of hydrogels in the light path results in occasional deviation from linear behavior, the overall trend shows the photocatalytic nature of the reaction. We note that no hydrogen was observed at all time points when the photoabsorber hydrogel was absent.

Supplementary Figures

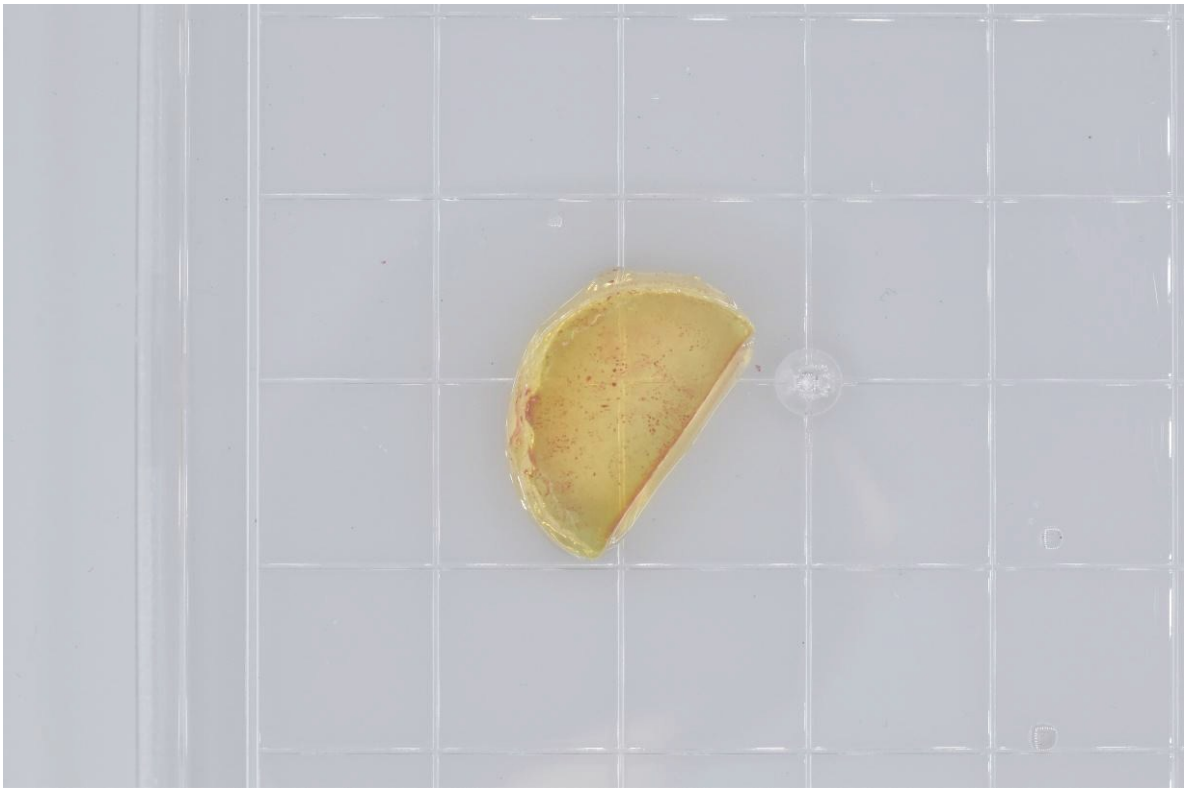

Figure S1. Photograph of a 1% crosslinker APTAC gel after immersion in PMI solution (10 mL of 0.5 mg/mL solution) overnight at 90^{o}C. The hydrogel was washed with water before photographing. The red dots are surface aggregated PMI residues. The yellow color of the bulk hydrogel, along with the presence of PMI aggregates in solution (not shown here), indicates that the amount of PMI incorporated in the bulk of the hydrogel is minimal even after accelerating diffusion at elevated temperature.

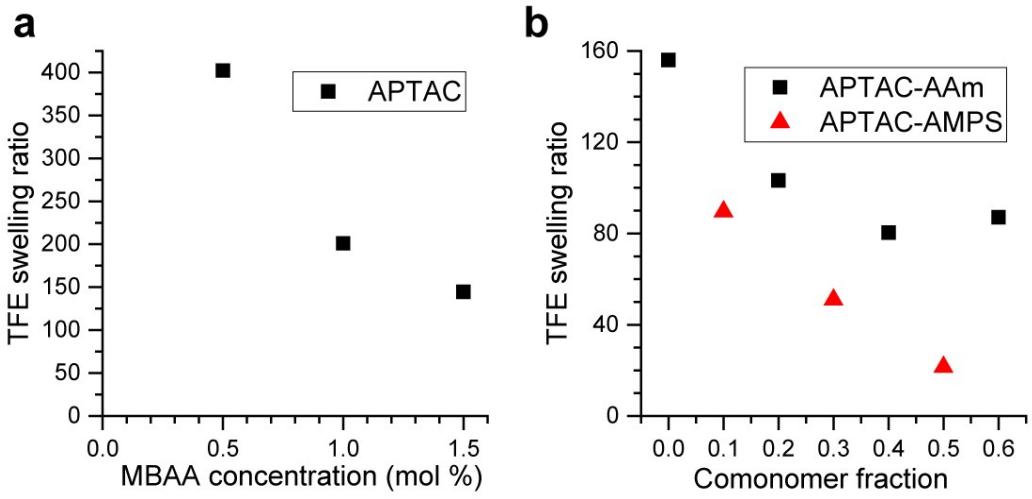

Figure S2. Swelling ratios of gels in trifluoroethanol, defined as weight of the TFE-swollen gel divided by the weight of the dried gel. (a) APTAC gels with varying crosslinker concentration. (b) APTAC/AAm and APTAC/AMPS copolymer gels at MBAA concentration of 1.5 %. The decrease in swelling ratios upon addition of comonomers indicate the reduced ability of these copolymer gels in TFE uptake.

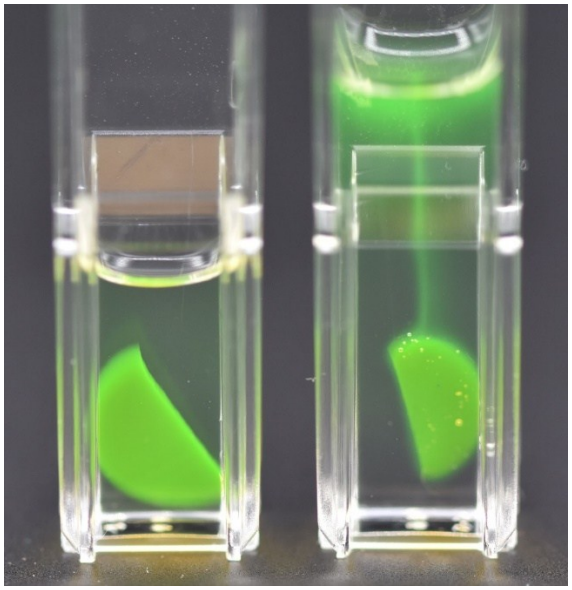

Figure S3. Photographs of fluorescein disodium salt-loaded APTAC hydrogels in DI water (left) and in 150 mM $NaCl_{aq}$ (right), 2 min after immersion in respective media, showing the dye leaching out of the hydrogel in high ionic strength condition. Loading of fluorescein was achieved via immersion of APTAC xerogels in 0.1 mM fluorescein aqueous solution. This result is in contrast to PMI/PE hybrid hydrogels in that PMI is retained upon exposure to salt solution.

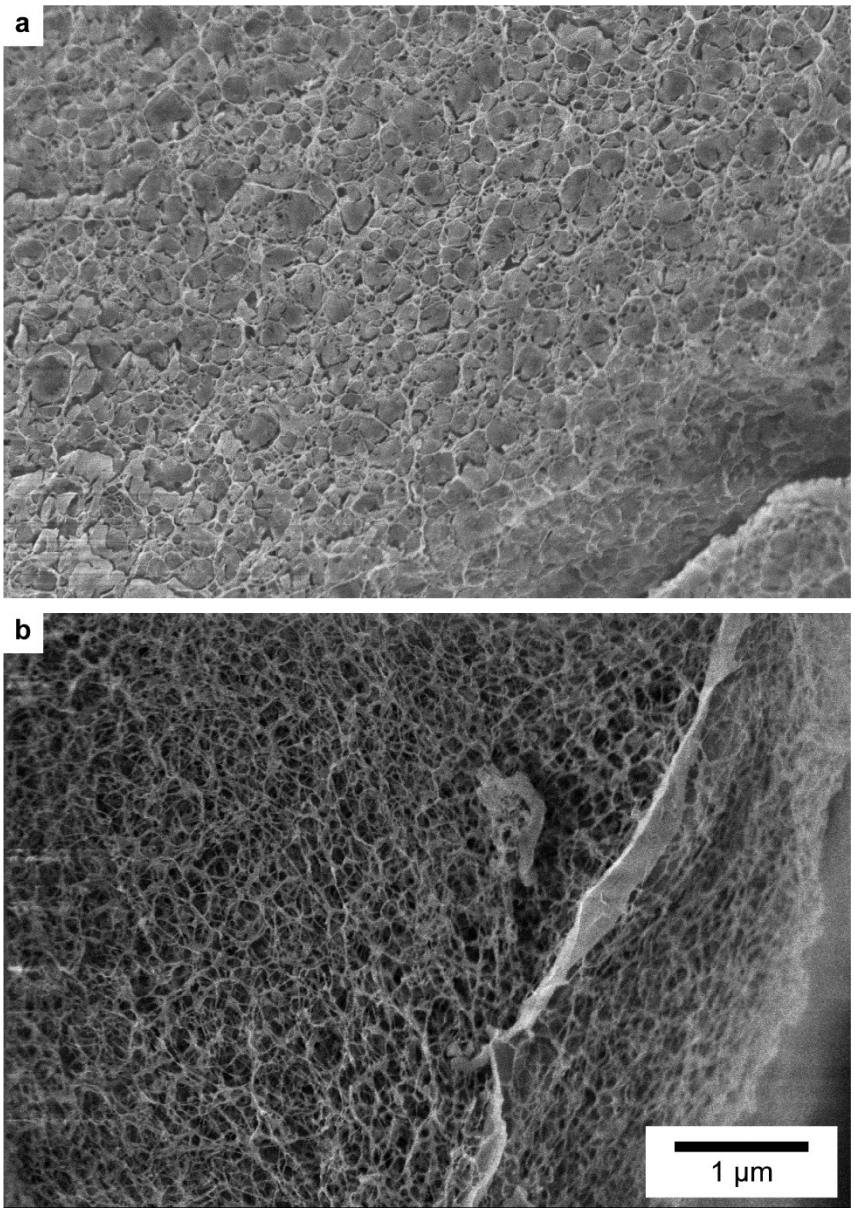

Figure S4. Cryo-SEM images of (a) the parent APTAC hydrogel and (b) the corresponding PMI/APTAC hybrid hydrogel, showing the network structure of the polyelectrolyte as well as the size comparison between the PMI ribbon (flat object on the right) versus the covalent network. The web-like structure represents the polymer, with the partially etched vitrified water occasionally filling the voids. The characteristic sizes of the polymeric network are smaller than the PMI feature sizes.

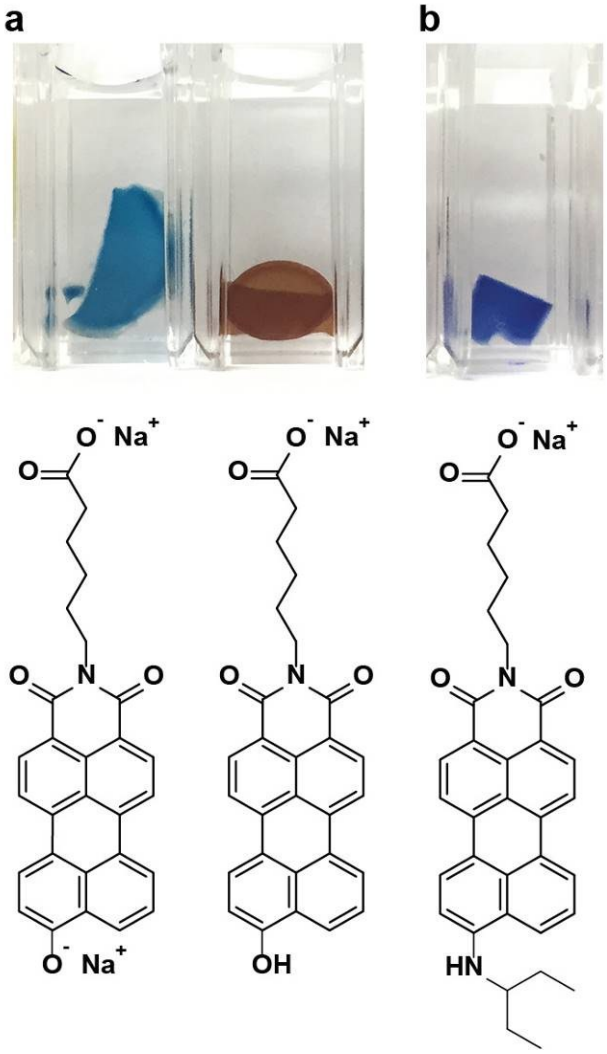

Figure S5. Photographs of CA/PE hybrid hydrogels from various chromophore amphiphiles and APTAC hydrogels and their respective CA molecular structures. (a) OH-functionalized PMI under basic (left, pH 10) and acidic (left, pH 4) conditions. (b) 3-pentylamine-functionalized PMI.

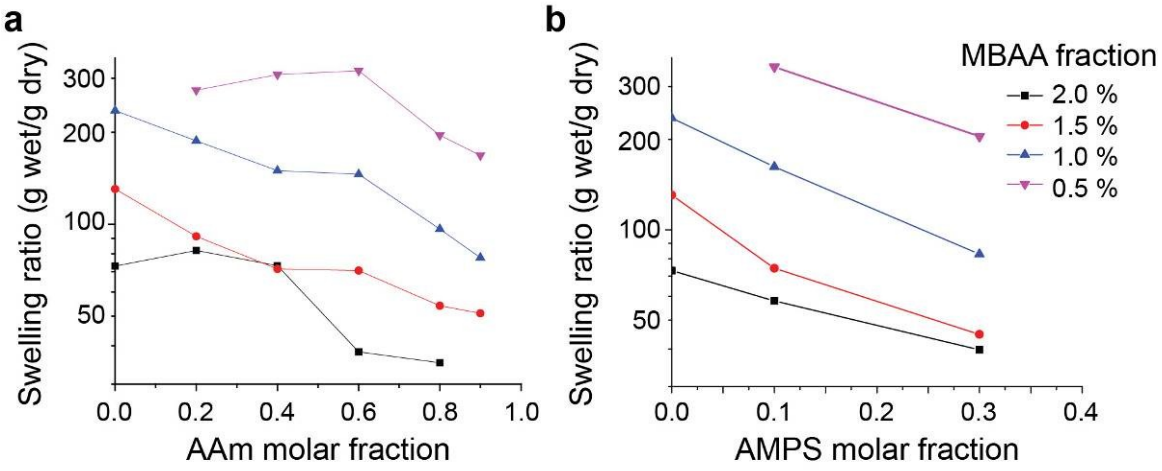

Figure S6. Swelling ratios of parent copolymer hydrogels in DI water with varying crosslinking densities. (a) AAm/APTAC copolymer hydrogels. (b) AMPS/APTAC copolymer hydrogels.

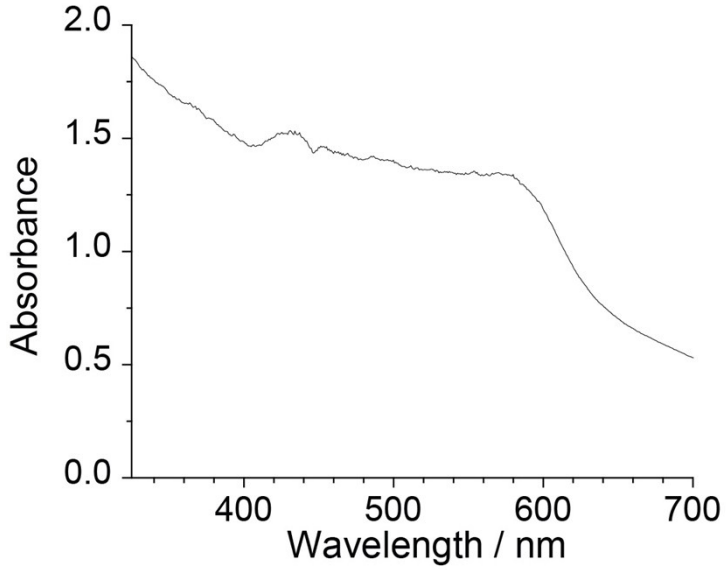

Figure S7. UV-Vis absorption spectra of PMI/APTAC hybrid hydrogel after thermal annealing in 150 mM $NaCl_{aq}$. The strong scattering signal is overlaid on the bimodal signature of the crystalline PMI absorption.

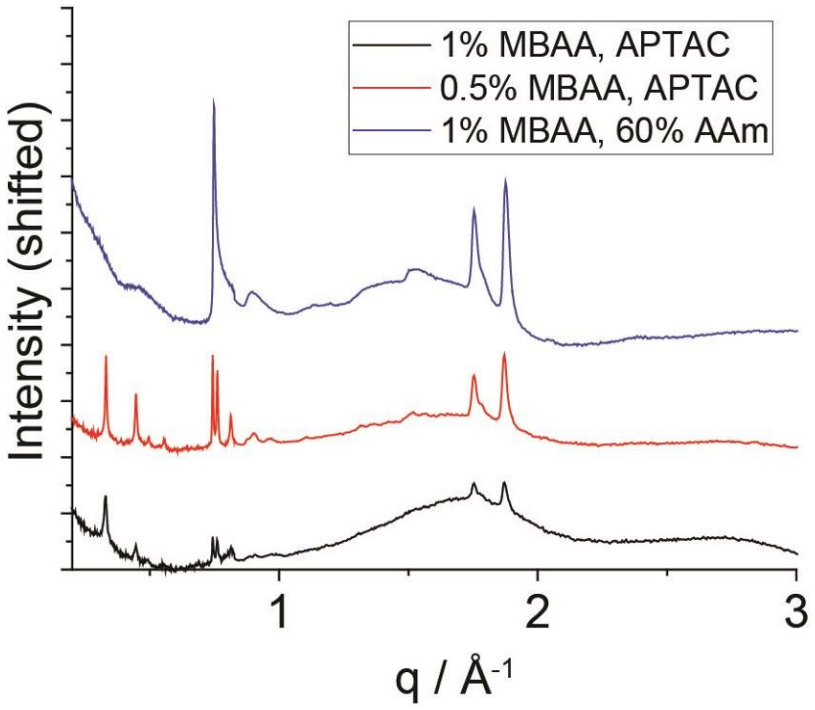

Figure S8. X-ray scattering profiles of PMI/PE hybrid hydrogels with varying parent hydrogel compositions, after annealing in 150 mM $NaCl_{aq}$. Note that for the hybrid hydrogel containing 60 mol% AAm, the stacking peaks observed in the middle angle regions are absent while the wide-angle peaks are stronger. This indicates that the PMI supramolecular structures may be more independent of the parent gel network.

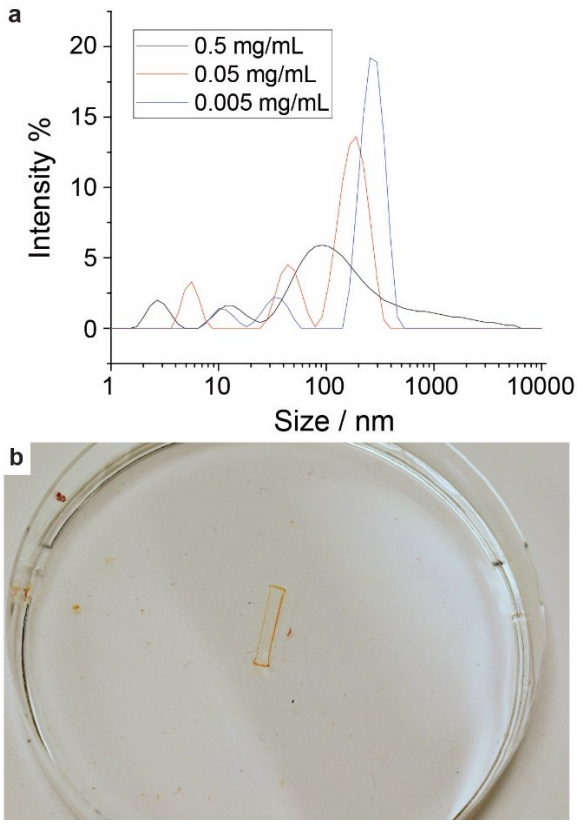

Figure S9. (a) Intensity-based size distribution plots of the $Na_2[Mo_3S_{13}]$ solution in water at varying concentration. Solutions were prefiltered with 0.2 μm filters before measurements. Multimodal size distribution indicates their tendency to cluster. (b) Cross-sectional photograph of the parent APTAC gel swollen in the molybdenum-sulfur cluster catalyst $Na_2[Mo_3S_{13}]$ solution. The orange/brown catalyst is shown to accumulate on the surface of the swollen hydrogel, and is not incorporated into the interior of the hydrogel.

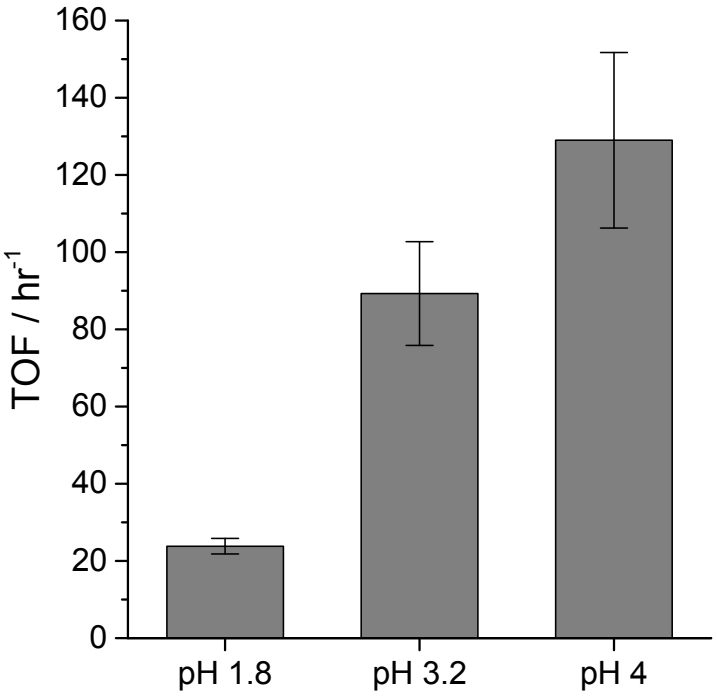

Figure S10. pH-dependent turnover frequency measurements for PMI/PDDA systems with $[Mo_3S_{13}]^{2-}$ in aqueous environment using ascorbic acid as the sacrificial electron donor. Ascorbic acid as dissolved at 2.5M in water shows a pH of around 1.8, and the pH 3.2 samples were pH-adjusted with half the amount of $NaOH_{aq}$ as the nominal pH 4 samples.

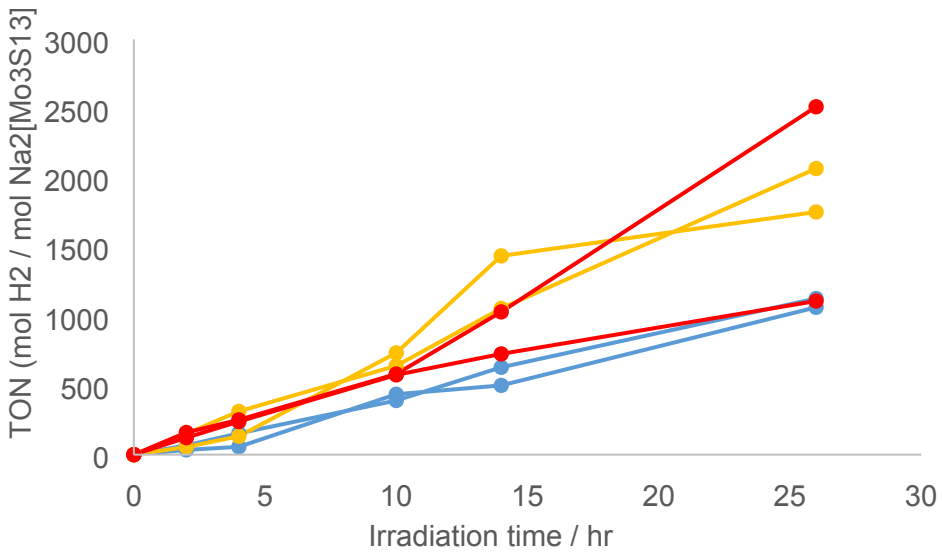

Figure S11. Kinetic data for photocatalytic hydrogen production. Each line corresponds to a data set taken from the same vial under irradiation at different times.

Supplementary Methods for Coarse-Grained MD Simulations

Coarse-grained (CG) simulations are performed in implicit solvent using LAMMPS Molecular Dynamics (MD) package.[1] All the charges of the chains constituting the hydrogel network as well as those on the perylene monoimide (PMI) molecules are considered explicitly together with their neutralizing counterions since explicit treatment of the counterions can affect the self-assembly kinetics.[2] In the simulations, the molecular weight between two hydrogel crosslinks, PMI concentration and ionic strength (i.e., screening length) are varied, and their effects on assembly properties of the hybrid systems are focused.

Hydrogel network

The hydrogel network is modeled as a three-dimensional defect-free cubic lattice composed of bead-spring polyion chains.[3,4] The chains are crosslinked permanently. The chemical details of the hydrogel backbone are described by a monomer size of 1σ and a charge fraction parameter of f=1 (i.e., all monomers are charged). The number of monomers between two crosslinks is N=30. The entire hydrogel polymer network is composed 27 nodes (i.e., 9 hydrogel unit cells). The polymer network is periodic in all directions (i.e., no dangling ends) and prepared in a stretched configuration prior to the minimization process (see below). The sizes of each monomer and counterions are set to a distance of 1σ (see next section for details). Note that this size is the reference size for other monomers that will be introduced throughout this work. The chains are initially prepared with initial bond length of 1σ. Each monomer of the chains carries a positive charge, including the crosslinking nodes. For each positive charge, a negatively charged monovalent counterion is added at a random position to ensure global electroneutrality in each simulation box.

PMI molecules

In the coarse-graining procedure of the PMI molecular structure, we focus on modeling the strong hydrophobic interactions between the aromatic groups and repulsive electrostatic interactions between the head groups of the PMI molecules. In general, our aggregates are insensitive to fine details of coarse-graining procedure (e.g., cutoff distances or energy scales) as long as the aforementioned strong attraction and repulsion are maintained in the models.

The atomistic PMI model is converted into a CG representation, in which the perylene area is represented by a 10-bead flat structure, and the head group is represented by a flexible tail consisting of two neutral beads and one negatively charged bead (See Figure S12 and Table S1 and S2). Each bead is categorized into one of the four types described in Table S1, where the relative strength of pair interaction parameters is constructed based on the Martini force field.[5] The bonded interactions, bond angles and improper dihedrals are represented by harmonic functions to keep the perylene area of the PMI molecule flat (see the next section for details). For bead sizes and charges, the hydrogel monomers are used as reference. The coarse grain model is validated by comparing the local molecular packing to atomistic model (Figure S13) as well as the experimental data (see the main text). All monomers composing the PMI molecules are neutral except the head group.

Interaction potentials

The excluded volume interactions between two monomers separated by a center-to-center distance r_{ij} is modeled by a shifted Lennard-Jones (LJ) potential

$$U_{LJ}(r_{ij}) = \begin{cases} 4\epsilon_{ij}\left(\left(\frac{\sigma_{ij}}{r_{ij}}\right)^{12} - \left(\frac{\sigma_{ij}}{r_{ij}}\right)^{6}\right), & r_{ij} < r_c \\ 0, & r_{ij} \geq r_{c,} \end{cases}$$

where σ_{ij} is the monomer diameter in reduced LJ units for respective *i-j* pair (if *i=j* otherwise see Table S2), and ϵ_{ij} is the reduced energy in the units of k_BT, where k_B is the Boltzmann constant, and T is temperature (see Table S2). The LJ potential is shifted at the cutoff radius to provide a continuous profile. The good solvent condition for the hydrogel and counterions is modeled by setting $r_c = 2^{1/6}\sigma_{ij} \approx 1.122\ \sigma_{ij}$ so only the repulsive part of the LJ potential remains.[4,6] The LJ potential is applied to all backbone-backbone interactions, backbone-ion interactions and ion-ion interactions with different set of σ values (see the next sections for parameters).

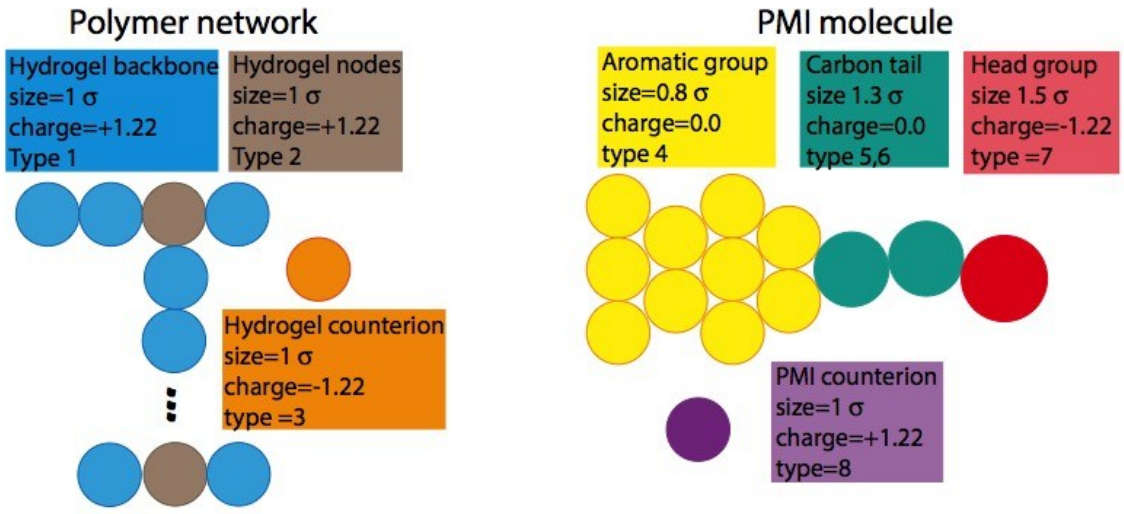

Figure S12: Parameters for the Coarse-grained models of the polymer network and PMI molecules. Refer Table 1 and 2 for monomer types and charges. The reference monomer size 1 σ for all structures. The units of charge are *e*.

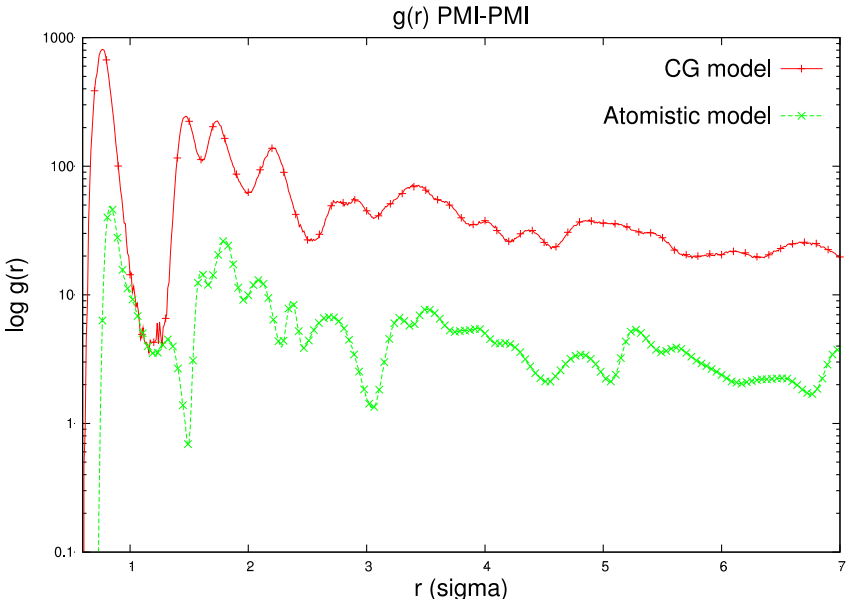

Figure S13: Comparison of the radial distribution functions (of center of mass of the aromatic sections) between the atomistic and coarse-grained descriptions of PMI molecules. The average packing and peak positions of the PMI molecules in the two approaches are consistent for the purpose of the current study.

The interaction between two bonded monomers of the polymer network is described by a FENE potential[4]

$$U_F(r_{ij}) = \begin{cases} -\frac{1}{2}k_F r_F^2 \ln\left(1 - r_{ij}^2/r_F^2\right), & r_{ij} < r_F \\ \infty, & r_{ij} \geq r_{F,} \end{cases}$$

where $k_F = 20\ k_B T/\sigma^2$ is the spring constant, and r_F=1.5 σ_{ij} is the maximum bond length. For the PMI molecules, instead of FENE, a harmonic potential ($k_F(r - r_F)^2$) with $k_F > 1000\ k_B T/\sigma^2$ to suppress any fluctuations.

For the PMI, to keep the molecules flat, a harmonic angle potential, $U_\theta \approx k_\theta(\theta - \theta_0)^2$, where the spring constant is $k_\theta =$ 50 k_BT/rad^2, and the two different reference angles are θ_0=150^o, 180^o, is used. In addition, a harmonic improper dihedral potential, $U_D \approx k_D(\chi - \chi_0)^2$, where the spring constant is $k_D =$ 400 k_BT/rad^2, and the reference dihedral angles formed by for atoms angles are χ_0=0^o is introduced to further enforce a flat structure.

The short-range electrostatic interactions are modeled by the pairwise Coulomb potential

$$U_C(r_{ij}) = -\epsilon\frac{l_B}{r_{ij}},\ r_{ij} < r_e$$

.

The strength of electrostatic interactions is characterized by Bjerrum length $l_B = e^2/4\pi\varepsilon_0\varepsilon k_BT$. Here, e is the unit charge; ε_0 is the vacuum permittivity, and ε is the relative permittivity of solvent and set to 1.0 in respective LAMMPS units. The Bjerrum length defines a length scale, beyond which the Coulombic interaction energies are less than the thermal energy k_BT. In simulations, the Bjerrum length is set as $l_B \approx 2\ \sigma \approx 7$Å, corresponding to water condition. The long-range Coulomb interaction in salt free systems is calculated via the PPPM algorithm, above the cutoff distance r_e>10 σ with a force accuracy of 10^{-4}.

In the cases, where the excess amount of salt screens the electrostatic interactions, an exponential decay factor is calculated for the interactions between all charged species for r_e < 6 σ as

$$U_C(r_{ij}) = -\epsilon\frac{l_B}{r_{ij}}e^{-\kappa r_{ij}},\ r_{ij} < r_e$$

.

where the inverse screening length $\kappa \approx 1.0\ \sigma^{-1}$ to account for the screening length imposed by the salt concentration of around 100 mM. Above $r_e > 6\ \sigma$, U_C is set to 0 due to short screening length provided by the high salt concentration.

MD procedure

The MD simulations are performed using LAMMPS simulation package.[1] The PMI molecules are randomly dispersed throughout the polymer network with their corresponding counterions. For each added PMI molecule, one hydrogel counterion is removed to keep the system charge neutral. Before obtaining data for analysis, first, an energy minimization procedure with a force tolerance of 10^{-8} is performed. Second, the system is integrated for 10^6 MD steps with microcanonical ensemble (constant monomer number N, constant volume V, constant total energy E), where a Langevin thermostat is applied at a reduced temperature of $T = 1.0$ with a damping parameter $\gamma = 1\ \tau^{-1}$, where τ is the LJ time scale, to keep the system temperature constant. The *NVE* integration provides further minimization and reduces steric overlapping among molecules. Third, following the *NVE* minimization, we perform few consecutive isothermal-isobaric (*NPT*) simulations, where the system pressure is set to P=0.0 to allow volume fluctuations in all dimensions with a pressure-damping parameter of $1.0\ \tau^{-1}$. In *NPT* simulations, the Nose-Hoover style non-Hamiltonian equations of motion are solved over all particles. All equilibration simulations are performed with MD time steps between Δt=0.0005 τ and 0.001 τ up to 10^6 MD steps. After the equilibration processes, the data production simulations are performed under *NPT* assemble. The production simulation is carried out with Δt = 0.002 τ up to 10^7 MD steps.

Temperature annealing procedure

The configurations that are obtained with salt free systems are heated up to a reduced temperature of T=3.0 at which most PMI aggregates are dissolved and form a gaseous phase. The heated systems, then, are brought to T=1.0 in 6 x 10^6 MD steps. The data collection runs are performed for an additional 1e+6 MD steps. The smaller annealing times are also checked, but no significant difference is observed in the final aggregates.

Type	Name	Size (units of □)	Charge (units of e)
1, 2	Hydrogel chains	1.0	+1.22
3	Hydrogel counterion	1.0	-1.22
4	PMI Aromatic group	0.7	0
5,6	PMI Hydrophobic tail	1.3	0
7	PMI head group	1.5	-1.22
8	PMI counterion	1.0	+1.22

Table S1: Types, group names, sizes and charges of the monomers constituting the hydrogel network and PMI molecules in the simulation models used in the simulations with LAMMPS MD package.

Pair (i-j)	σ_{ij} (units of σ)	ϵ_{ij} (units of $k_B T$)	r_c (units of σ)
4-4	0.70	1.50	6.0
4-5	0.98	0.95	1.122
4-6	1.30	0.95	6.0
4-7	1.50	1.05	1.122

5-5	1.30	1.0	6.0
5-6	1.30	1.0	1.122
5-7	1.50	1.1	6.0
6-6	1.30	1.0	6.0
6-7	1.50	1.1	1.122
7-7	1.50	1.2	6.0

Table S2: Pair interaction parameters for the LJ potential for the monomers constituting the PMI and hydrogel molecular structures that are obtained using Martini force field parameters. See Table 1 for the monomer types. If a pair is not defined above, σ_{ij}=1 σ, ϵ_{ij}=1 $k_B T$ and r_c=1.122 σ.

References:

1) Plimpton, S. *J. Comp. Phys.* **1995**, *117*, 1–19.
2) Erbas, A. de la Olvera Cruz, M., Marko, J. F., *Phys. Rev. E* **2018**, 97, 022405.
3) Erbas, A. de la Olvera Cruz, M. *ACS Macro Lett.* **2015**, *4*, 857–861.
4) Grest, G. S. Kremer, K. *J. Chem. Phys.* **1990**, *92*(8), 5057.
5) Marrink, S. J., Risselada, H. J., Yefimov, S., Tieleman, D. P., de Vries, A. H. *J. Phys. Chem. B* **2007**, *111*, 7812–7824.
6) Li, H., Erbas, A., Zwanikken, J., Olvera de la Cruz, M. *Macromolecules* **2016**, *49*, 9239–9246.